ACS OMEGA

Article

Cite This: ACS Omega 2018, 3, 1977−1982

Room-Temperature Ammonia Gas Sensing Using Mixed-Valent $CuCo_2O_4$ Nanoplatelets: Performance Enhancement through Stoichiometry Control

Srashti Jain,[†] Apurva Patrike,[†] Satish S. Badadhe, Monika Bhardwaj,* and Satishchandra Ogale*

Department of Physics and Centre for Energy Science, Indian Institute of Science Education and Research, Pune 411008, India

Supporting Information

ABSTRACT: We report the sensing properties of an interesting ternary oxide $CuCo_2O_4$ (CCO) which comprises two earth-abundant transition elements, both capable of supporting multiple valence states. We have used a synthesis protocol, which renders unique nanoplatelet-type morphology but with a degree of biphasic character (CuO as a secondary phase in addition to the defect-spinel $Cu_{1-x}Co_2O_4$). This sample constitution can be controlled through the use of cation off-stoichiometry, and the same also influence the sensing response significantly. In particular, a Co 10 at. % excess CCO (CCO−Co(10)) case exhibits a good response (~7.9% at 400 ppm) for NH_3 gas with a complete recovery at room temperature (23 °C, ±1 °C) in 57% RH. The material performance was investigated for other gases such as H_2S, NO_2, and CO. A good response is observed for H_2S and NO_2 gases but without a recovery; however, for CO, a poor response is noted. Herein, we discuss the specific results for ammonia sensing for the CCO−Co(10) case in detail via the use of different characterizations and outline the difference between the cases of the single-phase defect-stabilized material versus nonpercolating biphasic material.

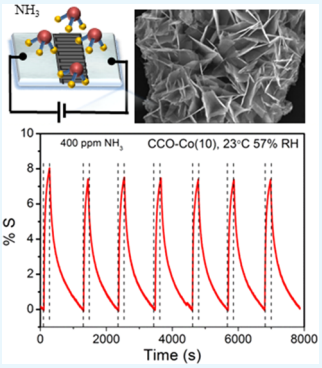

INTRODUCTION

Rapid technological and industrial developments continuously result in the emission of hazardous gases, toxins, and biomolecules. Therefore, sensing of such undesirable chemical or biochemical forms has become a significant research endeavor in recent years.[1−3] Certain gases such as NH_3, NO_x, and CO are contributed to the atmosphere regularly in significant quantities by transportation and chemical industries, which have a deteriorating influence on the environment in various ways.[4] Issues of safety and security also hinge upon detection of trace elements of chemical agents. Some of these pollutants are extremely dangerous, and hence sensing them at ppm levels is crucial for the harmonious survival of mankind as well as the ecosystem at large.

Different materials and detection schemes have been adopted in this context to achieve high responsivity combined with less response/recovery time, which are key quality factors that define the sensor performance. In particular, oxides are extensively researched for gas sensing, in view of their robust material properties and their ability to change valence through charge transfer.[5−7] Several binary oxides have been examined for effective gas sensing and have yielded promising results.[5−13] The interaction of analyte gas molecules depends on the surface atoms present in the metal oxides. The catalytic activity of metal oxides depends on the relative acidic and basic character of the atoms present on the surface which is affected by coordination between the metal atom and oxygen anions. In the case of binary metal oxides, the accessible property regimes in this respect are rather limited. On the other hand, in the case of ternary metal oxides, there are two acidic sites and one basic site; hence, the multitude of their interactions renders wider property windows for the catalytic performance. However, the ternary oxide and sulfide systems, which offer distinct advantages of stoichiometry and valence control, are relatively less explored by far.[14−27]

Herein, we report the sensing properties of an interesting ternary oxide $CuCo_2O_4$ (CCO) which comprises two earth abundant transition elements, each having an ability to support multiple valence states (Cu 1+ and 2+ and Co 2+ and 3+).[28−30] Although the sensing performance of CCO at a high temperature of 300 °C is already reported,[26] its effective gas-sensing response at room temperature is hitherto unexplored. In the present study, we have successfully shown that a controlled stoichiometry manipulation and porous nanoplatelet morphology of CCO were responsible for superior gas-sensing activity for ammonia gas at room temperature.

RESULTS AND DISCUSSION

Characterization of the Gas-Sensing Material. A detailed description of the synthesis and characterization of the three different materials, viz., CCO, CCO−Cu(10), and CCO−Co(10) is reported in our previous publication.[28] It was envisaged to achieve porous nanoplatelet morphology of the material that would facilitate effective gas adsorption on account of the enhanced surface area for higher surface

Received: December 8, 2017
Accepted: February 5, 2018
Published: February 15, 2018

DOI: 10.1021/acsomega.7b01958
ACS Omega 2018, 3, 1977−1982

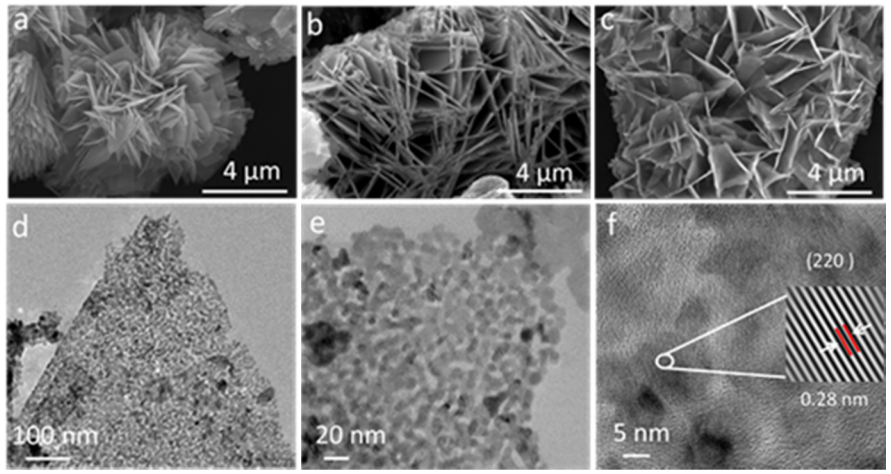

Figure 1. FESEM images of (a) CCO, (b) CCO−Cu(10), and (c) CCO−Co(10) and HRTEM images of CCO−Co(10) at different scales (d) 100, (e) 20, and (f) 5 nm.

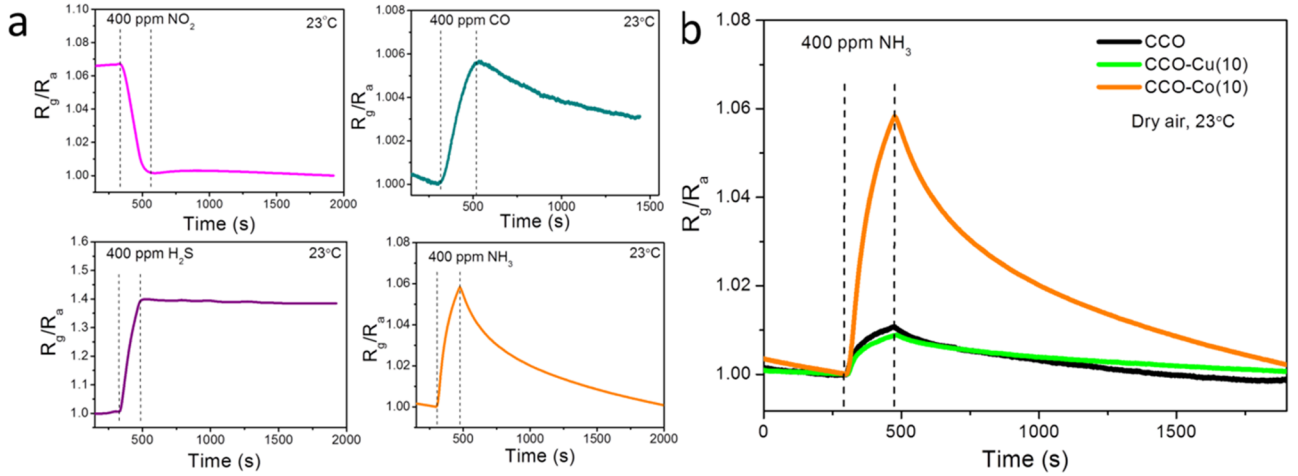

Figure 2. (a) Gas-sensing response of CCO−Co(10) toward 400 ppm of different gases NO_2, CO, H_2S, and NH_3 at 23 °C in dry air. (b) Ammonia-sensing measurements for different stoichiometries of CCO at 23 °C in dry air.

accessibility, the proper range of conductivity, and higher density of surface defects. Although there are numerous methods to obtain a single-phase CCO starting with a stoichiometric mixture of precursors; however, these do not yield the appealing morphology of interest required for different applications such as battery electrodes and sensor elements.[26,28−34] In the current study, it was observed that the hydrothermal synthesis route using a stoichiometric mixture of precursors resulted in a product with the desired morphology but with an undesirable secondary phase. As seen in Figure S2a, the powder product consists of a copper-deficient defect-spinel phase of CCO along with a minor secondary phase of CuO. Hence, to suppress this secondary phase, the synthesis was performed with an off-stoichiometric precursor mixture with excess cobalt. It was found that 10 at. % excess cobalt in the precursor mixture leads to a single-phase sample with almost a negligible secondary CuO phase. It means that the nearly single-phase sample formed has excess cobalt, so by implication, it is also a defect spinel but a single phase. Separately, we also examined the case of excess copper added to the precursor to enhance the CuO component so as to obtain a CuO/defect−CCO composite in the context of another application interest. This gave us an opportunity to examine all these three materials, which represent interesting sample states in terms of the phase constitution, defects states, and biphasic versus single phase nature for the sensing application. In the following section, we give some relevant characterization results performed on the new set of samples used specifically in this work.

Figure 1a−c shows the field emission scanning electron microscopy (FESEM) images of the three cases of interest, namely CCO, CCO−Cu(10), and CCO−Co(10). The morphology generally appears to be in the form of flower-like nanoplatelets which cross one another. Thus, the off-stoichiometry does not make major changes in the morphology. The high-resolution transmission electron microscopy (HRTEM) data of Figure 1d,e reveal that the platelets are assembled through nanoparticles of a rather uniform size of about 10−15 nm via oriented attachment as suggested by their planar assembly with nanoporosity throughout. Figure 1f shows lattice fringes with a *d*-spacing of 0.28 nm, which matches well with the (220) plane of CCO. Thus, the nanoporous nature of these nanoplatelets is essential for the sensing application because it provides better access and high surface area for the adsorption of the analyte gas.

DOI: 10.1021/acsomega.7b01958
ACS Omega 2018, 3, 1977−1982

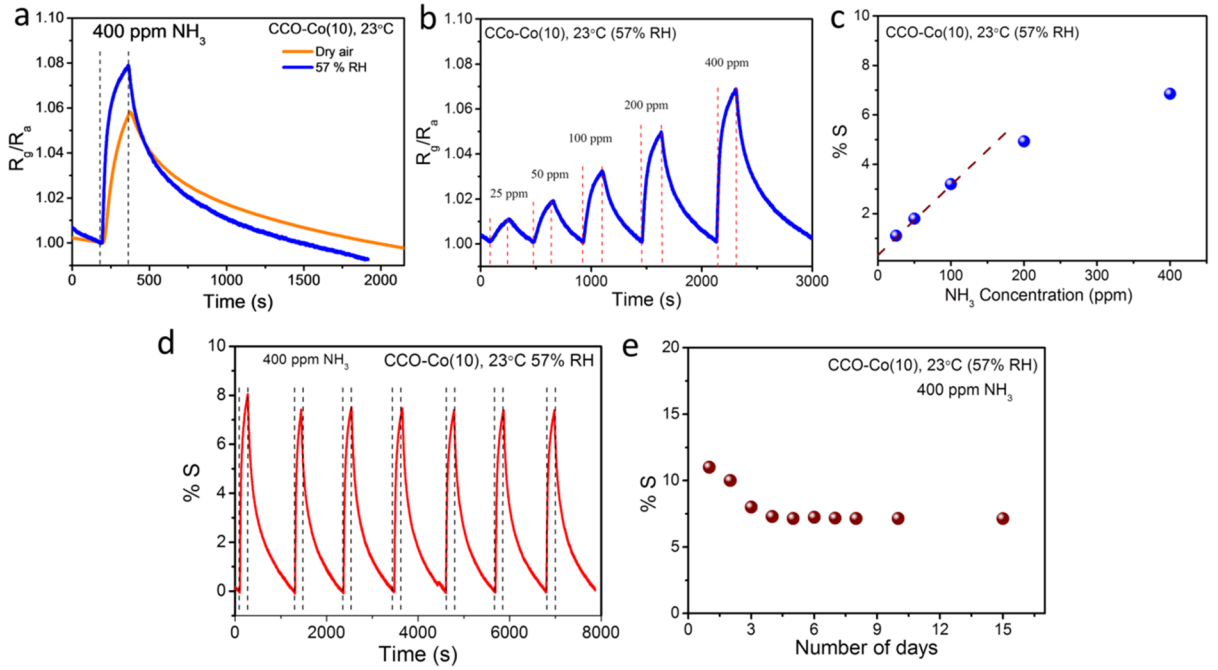

Figure 3. (a) ammonia sensing of CCO−Co(10) in dry air and 57% RH at 23 °C; (b) response of CCO−Co(10) toward different concentrations of NH_3; and (c) its relation between % *S* with NH_3 concentration in 57% RH at 23 °C. (d) Dynamic response of CCO−Co(10) toward ammonia for different cycles of 400 ppm in 57% RH at 23 °C. (e) Stability of CCO−Co(10) toward 400 ppm NH_3 in 57% RH at 23 °C.

Sensor Response. First, the gas-sensing behavior of the CCO−Co(10) material for different gases at room temperature was investigated, and the resultant data are shown in Figure 2a. The exposure time for the analytic gas was kept fixed at 3 min. The CCO−Co(10) powder coating used for gas sensing was drop casted on a glass substrate, and corresponding X-ray diffraction (XRD) is shown in Figure S2b. Basically, it represents the same XRD as that of the CCO−Co(10) powder material. It was found that the material senses all the gases, but it shows recovery only for the case of NH_3. In the presence of reducing gases such as NH_3, H_2S, and CO, the resistance was increased, whereas in the presence of oxidizing gas (such as NO_2), there was a reduction in the resistance of CCO−Co(10). This confirms the p-type nature of CCO Co(10).[34−36] As reported above, CCO with their nanotube morphology was implemented for gas sensing at a high temperature of 300 °C for a few target gases.[26] Although, it is clear that the other gases interact nonreversibly (at least over the time scale examined) with the sample (Figure 2); however, the novelty of our work lies in the fact that gas sensing is being carried out at room temperature. Because both the elements in this ternary system, viz., Co and Cu, exist in two valence states, it is not entirely surprising that the material will respond to reducing as well as oxidizing gases. The recovery being an important consideration in a sensing application, further work was mainly focused on NH_3 sensing. The statements made here about the sensing of different gases are broadly valid for CCO and other off-stoichiometric cases also.

Figure 2b shows NH_3 gas-sensing properties of all three composites in dry air as carrier gas at 23 °C. It can be seen from Figure 2a that at room temperature, the CCO−Co(10) sample (single-phase defect spinel) showed a much superior response toward NH_3 gas as compared to the CCO and CCO−Cu(10) biphasic samples. The CCO−Co(10) exhibits gas response of ∼6% at 400 ppm of NH_3. There could be three key reasons for this observation of superior performance by a single-phase material as compared to the other two cases, which are in a composite state. First is the potential competition for gas adsorption sites between the two phases depending on the adsorption chemistry; second is the potential siphoning of active carriers to the interface traps between the two constituent phases making them ineffective for transport. Last is the transfer of the carrier to the secondary phase rendering them unavailable for transport because of percolation issues. Further work will be needed to elucidate and separate out these issues.

Therefore, on the basis of the high sensitivity of CCO−Co(10) to NH_3 at room temperature (23 °C), further detailed gas-sensing studies were performed on this CCO−Co(10) material. For practical application, it is necessary to determine gas-sensing properties of the sensor at room temperature, and for this condition, the sensor performance is greatly influenced by the surrounding humidity as well. Hence, measurements were performed in a practically typical relative humidity condition (∼57% RH). Figure 3a shows NH_3-sensing behavior of CCO−Co(10) in the presence of 57% RH and dry air at 23 °C. It can be seen that the sensor exhibits enhanced response in the presence of 57% RH as compared to dry air. Importantly, the recovery time is also reduced in the humid atmosphere (14 min compared to 18 min in dry air). The enhanced response in the humid environment suggests that in the presence of humidity, NH_3 reacts with H_2O forming NH^{4+} and OH^-, which facilitates the interaction with the sensor.[37] Therefore, concentration-dependent NH_3 response, cyclic reproducibility, and also the device stability over the period were carried out in 57% RH at room temperature.

Figure 3b shows the response of CCO−Co(10) over the concentration range from 25 to 400 ppm of NH_3 in 57% RH at room temperature. Also, the response as a function of NH_3 gas concentration was noted to be linear up to about 100 ppm suggesting nonsaturation of the active sites over this full range

DOI: 10.1021/acsomega.7b01958
ACS Omega 2018, 3, 1977−1982

(Figure 3c). At higher concentrations, however, saturation is noted from the departure from linearity.

Figure 3d shows the performance repeatability of CCO−Co(10) exposed to 400 ppm NH_3 in 57% RH over seven cycles. A small decrease in the response is noted after one cycle, which can be attributed to the leftover analyte gas on the surface of the material from the previous cycle. However, after the first cycle, the device exhibits quite a stable gas response. We have also investigated the stability of CCO−Co(10) over a period of 15 days (Figure 3e) and observed that there is a slight gradual drop in the response over the first couple of days, but the response remains relatively constant over the period of 15 days. This suggests a robust gas-sensing performance of the CCO−Co(10) sensor at room temperature in a humid atmosphere (57% RH).

Table S1 compares the response of CCO−Co(10) to NH_3 with other metal oxide semiconductors. It is evident that CCO−Co(10) renders fairly good gas response values with fast response and lower optimal operating temperature comparable or better than other sensing materials.

In general, the sensing properties of metal oxide-based gas sensors depend on many factors such as surface area, microstructures, defect levels, and so forth. The detailed gas-sensing mechanism is incorporated in the Supporting Information. Figure S4 shows schematic illustration of the gas-sensing mechanism in the presence of reducing and oxidizing gases.

To systematically understand the observed gas-sensing data at room temperature, it is essential to discuss the microstates of the three samples examined, namely CCO, CCO−Co(10), and CCO−Cu(10). As discussed in our previous paper at some length, under the specific hydrothermal growth conditions used to achieve the peculiar platelet-like morphology for the benefit of higher surface area and accessibility, the use of the stoichiometric mixture of precursors leads to a mixed phase; wherein, a small quantity of CuO is present as a secondary phase in addition to the main CCO phase, which is naturally Cu-deficient.[28] Other reports have also discussed the occurrence of the secondary CuO phase.[31−34,38,39] When an excess cobalt precursor is included in the synthesis vessel, the contribution of the secondary CuO phase diminishes, and at about 10% excess Co, an almost single-phase sample is realized. It must be borne in mind, however, that this single phase is also a defect-spinel phase because it is richer in cobalt than the basic CCO stoichiometry. It is possible that in this case the charge balance will be enforced via a change in the oxygen stoichiometry. Separately, when excess Cu is added in the precursor mixture, it can play a dual role. It could simply add to the separated CuO secondary component or partially eliminate the Cu vacancies. This could again lead to a defect-stabilized CCO phase with a different density of defect types as compared to the other two cases. Thus, it is hard to precisely compare the three cases, although some compelling arguments can be made, particularly in the context of the observed much stronger response of CCO−Co(10) to ammonia as compared to the other two biphasic cases.

The Brunauer−Emmett−Teller (BET) surface area measurements were performed on the three samples to examine whether the initial precursor stoichiometry differences affect the surface area significantly, which in turn influences the sensor performance (Figure S3). It can be seen that the surface area of CCO, CCO−Cu(10), and CCO−Co(10) was 45, 50, and 55 m^2/g, respectively; and hence, they do not differ that significantly. However, there will be a little contribution of increased surface area on gas response in CCO−Co(10). To further establish the chemiresistive sensing results, the powders were pelletized to study their bulk electrical conductivity. It was observed that the conductivity was lowest for the CCO−Co(10) case, followed by the CCO−Cu(10) case, and then the CCO case. Because the three-dimensional percolation threshold for the secondary phase to make a major influence on the transport is 18%, in both the cases of CCO and CCO−Co(10), the secondary CuO phase is nonpercolating. Thus, the transport is primarily dominated by the defect-spinel CCO component, and the differences in the defect-borne electronic states in the three cases are responsible for the observed resistivity data. The conductivity (resistivity) is lowest (highest) for the CCO−Co(10) case as compared to those of the other two cases involving the presence of the secondary CuO phase in the form of nonpercolating distributed nanoscale regions. It suggests that this secondary phase may have a role in reducing the interface trap density and hence scattering. The changes in conductivity (resistivity) of the three samples are, however, not as significant as the ammonia sensitivity difference reflected by the CCO−Co(10) case sample vis-a-vis the other two cases. Thus, the search for the origin of this effect has to be sought in another argument.

In the two cases of CCO and CCO−Cu(10), wherein the secondary CuO phase is present, it would presumably occupy some grain boundary space and will also produce hetero-interfaces. When the sensing gas (NH_3) is introduced, it will be adsorbed on the surfaces of both the major CCO defect-spinel phase and the secondary CuO phase. The electron donated by the sensing gas will influence the conductivity of the material, which will be decided by the possibility of the transfer of this electron to the major phase because the secondary phase cannot by itself percolate. Our observation of much lower response to ammonia for the biphasic cases implies that there is a hindrance to the carrier transfer process between the major and secondary phases. This hindrance could occur by the band alignment and/or presence of interface trap states. The observed low response in the biphasic composites as compared to the CCO−Co(10) case could also be explained based on the hard soft acid base (HSAB) theory. In these composites, copper is in the form of Cu^{2+}, which is a borderline acid; however, cobalt is in the form of Co^{3+}, which is a hard acid. The reducing gas NH_3 is a hard base. According to HSAB theory, hard acid prefers hard base; therefore, in the present case, the Co^{3+} site is comparatively active toward the NH_3 gas compared to Cu^{2+}. As discussed earlier, in the CCO case, CuO emerges as the impurity phase, and the resulting surface contribution of this weak sensing phase will be counterproductive for sensor performance. In the CCO−Cu(10) case, this problem may get accentuated further.

In the case of the nanosystem at hand, the unavailability of information regarding the precise defect and interface states precludes a full understanding of the observed effects at this time. However, a message emerges that use of nanocomposites, formed intentionally or unintentionally, especially in the nonpercolating regime for the secondary phase, involves complex considerations and cannot always ensure an enhanced response.

CONCLUSIONS

A ternary oxide, namely CCO, with two multivalent transition elements, is examined for its chemiresistive properties. Unique

DOI: 10.1021/acsomega.7b01958
ACS Omega 2018, 3, 1977−1982

nanoplatelet-type morphology is realized by the specific choice of the synthetic protocol, but it intrinsically leads to a biphasic state (CuO as a secondary phase in addition to the defect-spinel $Cu_{1-x}Co_2O_4$). Employing a degree of cation off-stoichiometry, the constitution of the sample is controlled, and the sensing response is found to be modified accordingly. Three cases, viz., 10 at. % excess Co with CCO, 10 at. % excess Cu with CCO, and the right stoichiometric precursor ratios are examined. In particular, a Co 10 at. % excess CCO (CCO−Co(10)) case exhibits a good response (~7.9% at 400 ppm) for NH_3 gas with a complete recovery in 57% RH at 23 °C. Although the material exhibited a good response (without any recovery) for H_2S and NO_2 gases, the sensing performance was found to be poor in the case of CO. These observations are attributed primarily to the differences in the character of the carrier transport between the cases of the single-phase defect-stabilized material versus the nonpercolating biphasic material.

EXPERIMENTAL SECTION

Material Synthesis. The CCO sample was synthesized by a simple hydrothermal route. All the chemicals used in the present study were of analytical grade. The $Cu(NO_3)_2{\cdot}3H_2O$ (>99%) powder was obtained from Merck, whereas $Co(NO_3)_2{\cdot}6H_2O$ (>99%) and urea were obtained from LabChem. Initially, copper and cobalt precursors were mixed in deionized (DI) water in 1:2 molar ratio followed by the addition of 0.1 M urea to the solution. This was allowed to stir for 30 min under ambient conditions. The solution thus obtained was transferred into a 160 mL Teflon-lined autoclave and was heated at 120 °C for 16 h. The resultant black-colored solution was washed with DI water and then dried at 80 °C for 6 h. The final product was annealed at 350 °C for 2 h to obtain the desired phase and constitution of CCO. The same procedure was followed for preparing CCO samples with different cation stoichiometry ratios of copper and cobalt in the precursor mixture, namely copper excess case of CCO−Cu (10 at. % excess) and cobalt excess case of CCO−Co (10 at. %. excess).

Characterization. The required phase formation of the material was elucidated from powder XRD measurements that were carried out on a Philips X'Pert PRO diffractometer with nickel-filtered Cu Kα radiation (λ = 1.5418 Å). The diffractograms were recorded at a scanning rate of 1° min^{-1} between 10° and 80°. The morphology of the material was established using a high-resolution field emission Nova NanoSEM system. HRTEM (FEI Tecnai G2, F30 TEM microscope operating at an accelerating voltage of 300 kV) was also used for atomistic microstructural elucidation. The gas adsorption experiment (up to 1 bar) was performed on Quantachrome Autosorb-automated gas sorption analyzer.

Gas-Sensing Device Fabrication and Measurements. The gas-sensing setup is depicted in Figure S1a,b. An interdigitated (ID) pattern was developed on indium tin oxide (ITO)-coated glass with a CO_2 laser scriber. A fine paste was made by grinding the as-synthesized CCO powder along with a polyvinylidene fluoride binder and 2-propanol as a solvent. This paste was deposited on the ID-patterned ITO glass by doctor blading and maintained at 150 °C for 2 h. The film was mounted on the alumina plate and placed inside a chamber. Constant dc voltage of 2 V was applied across the film and current was measured by a Keithley 2400 source meter. We used cylinders of test gases with 0.1% of test gas balanced in nitrogen. The desired concentration of the test gas was obtained by controlling mass flow rates of the specific test gas and dry air. The gas-sensing measurements were carried out at 250 sccm of dry air. The gas response was measured at 23 °C in dry air. Because at room temperature the humidity can also affect the gas-sensing performance, the gas-sensing measurements were also carried out in 57% RH at 23 °C. The gas response (S) of the p-type sensor is defined as the ratio of the resistance in the presence of gas (R_g) to the resistance in the presence of air (R_a).

$$S = R_g/R_a \text{ (for reducing gas/oxidizing gas)}$$

where, R_a and R_g are the resistance of the sensor in air and gas, respectively. Relative percentage response is defined as $\% S = |R_g - R_a|/R_a \times 100$. Other important parameters such as response time and recovery time were also determined from the gas-sensing experiments. It is useful to mention here that it was difficult to achieve a perfect steady state in our case, and hence to control the experimental time, we had to accept a small drift in current before letting the sensing gas in for the measurement. Therefore, the response data are not included for extremely tiny concentrations of gas (e.g., 10 ppm), for which there is a chance of a small degree of ambiguity regarding the precise value of response.

ASSOCIATED CONTENT

Supporting Information

The Supporting Information is available free of charge on the ACS Publications website at DOI: 10.1021/acsomega.7b01958.

Schematic of the gas-sensing setup; XRD data; BET graphs and pore size distribution of CCO, CCO−Co(10), and CCO−Cu(10); comparative analysis of gas-sensing response of different materials; and discussion and schematic of the gas-sensing mechanism (PDF)

AUTHOR INFORMATION

Corresponding Authors

*E-mail: bharadwajmonika03@gmail.com (M.B.).
*E-mail: satishogale@iiserpune.ac.in, satishogale@gmail.com (S.O.).

ORCID

Satishchandra Ogale: 0000-0001-5593-9339

Author Contributions

†Equal contribution (S.J. and A.P.).

Notes

The authors declare no competing financial interest.

ACKNOWLEDGMENTS

S.S.B. would like to thank SERB-DST for national postdoctoral fellowship. The authors would like to thank the funding support for this work by the Board of Research in Nuclear Sciences (BRNS), Department of Atomic Energy (DAE), Government of India, and the DST Nanomission (Thematic Unit).

REFERENCES

(1) Wetchakun, K.; Samerjai, T.; Tamaekong, N.; Liewhiran, C.; Siriwong, C.; Kruefu, V.; Wisitsoraat, A.; Tuantranont, A.; Phanichphant, S. Semiconducting Metal Oxides as Sensors for Environmentally Hazardous Gases. *Sens. Actuators, B* **2011**, *160*, 580−591.

(2) Zhang, J.; Qin, Z.; Zeng, D.; Xie, C. Metal-Oxide-Semiconductor Based Gas Sensors: Screening, Preparation, and Integration. *Phys. Chem. Chem. Phys.* **2017**, *19*, 6313−6329.

DOI: 10.1021/acsomega.7b01958
ACS Omega 2018, 3, 1977−1982

(3) Korotcenkov, G. Metal Oxides for Solid-State Gas Sensors: What Determines Our Choice? *Mater. Sci. Eng., B* **2007**, *139*, 1−23.
(4) Rothschild, A.; Komem, Y. The Effect of Grain Size on the Sensitivity of Nanocrystalline Metal-Oxide Gas Sensors. *J. Appl. Phys.* **2004**, *95*, 6374−6380.
(5) Barsan, N.; Koziej, D.; Weimar, U. Metal Oxide-Based Gas Sensor Research: How To? *Sens. Actuators, B* **2007**, *121*, 18−35.
(6) Wang, Q.; Li, X.; Liu, F.; Liu, C.; Su, T.; Lin, J.; Sun, P.; Sun, Y.; Liu, F.; Lu, G. The Enhanced CO Gas Sensing Performance of Pd/SnO_2 Hollow Sphere Sensors under Hydrothermal Conditions. *RSC Adv.* **2016**, *6*, 80455−80461.
(7) Wang, C.; Yin, L.; Zhang, L.; Xiang, D.; Gao, R. Metal Oxide Gas Sensors: Sensitivity and Influencing Factors. *Sensors* **2010**, *10*, 2088−2106.
(8) Fine, G. F.; Cavanagh, L. M.; Afonja, A.; Binions, R. Metal Oxide Semi-Conductor Gas Sensors in Environmental Monitoring. *Sensors* **2010**, *10*, 5469−5502.
(9) Rai, P.; Khan, R.; Raj, S.; Majhi, S. M.; Park, K.-K.; Yu, Y.-T.; Lee, I.-H.; Sekhar, P. K. Au@Cu2O Core−shell Nanoparticles as Chemiresistors for Gas Sensor Applications: Effect of Potential Barrier Modulation on the Sensing Performance. *Nanoscale* **2014**, *6*, 581−588.
(10) Dong, C.; Wang, L.; Chen, G.; Xiao, X.; Djerdj, I.; Wang, Y. Facile Synthesis of CuO Micro-Sheets over Peeling off Cu Foil in Oxalic Acid Solution and Their Sensing Properties towards N-Butanol. *J. Mater. Chem. C* **2016**, *4*, 985−990.
(11) Cao, A.-M.; Hu, J.-S.; Liang, H.-P.; Song, W.-G.; Wan, L.-J.; He, X.-L.; Gao, X.-G.; Xia, S.-H. Hierarchically Structured Cobalt Oxide (Co3O4): The Morphology Control and Its Potential in Sensors. *J. Phys. Chem. B* **2006**, *110*, 15858−15863.
(12) Li, C. C.; Yin, X. M.; Wang, T. H.; Zeng, H. C. Morphogenesis of Highly Uniform CoCO3 Submicrometer Crystals and Their Conversion to Mesoporous Co3O4 for Gas-Sensing Applications. *Chem. Mater.* **2009**, *21*, 4984−4992.
(13) Li, X.; Wei, W.; Wang, S.; Kuai, L.; Geng, B. Single-Crystalline α-Fe2O3 Oblique Nanoparallelepipeds: High-Yield Synthesis, Growth Mechanism and Structure Enhanced Gas-Sensing Properties. *Nanoscale* **2011**, *3*, 718−724.
(14) Li, Z.; Wang, N.; Lin, Z.; Wang, J.; Liu, W.; Sun, K.; Fu, Y. Q.; Wang, Z. Room-Temperature High-Performance H $_2$ S Sensor Based on Porous CuO Nanosheets Prepared by Hydrothermal Method. *ACS Appl. Mater. Interfaces* **2016**, *8*, 20962−20968.
(15) Jiang, H.; Hu, J.; Gu, F.; Shao, W.; Li, C. Hydrothermal Synthesis of Novel In2O3 Microspheres for Gas Sensors. *Chem. Commun.* **2009**, 3618.
(16) Rai, P.; Majhi, S. M.; Yu, Y.-T.; Lee, J.-H. Noble Metal@metal Oxide Semiconductor Core@shell Nano-Architectures as a New Platform for Gas Sensor Applications. *RSC Adv.* **2015**, *5*, 76229−76248.
(17) Ou, J. Z.; Ge, W.; Carey, B.; Daeneke, T.; Rotbart, A.; Shan, W.; Wang, Y.; Fu, Z.; Chrimes, A. F.; Wlodarski, W.; Russo, S. P.; Li, Y. X.; Kalantar-Zadeh, K. Physisorption-Based Charge Transfer in Two-Dimensional SnS2 for Selective and Reversible NO2 Gas Sensing. *ACS Nano* **2015**, *9*, 10313−10323.
(18) Dai, Z.; Lee, C.-S.; Kim, B.-Y.; Kwak, C.-H.; Yoon, J.-W.; Jeong, H.-M.; Lee, J.-H. Honeycomb-Like Periodic Porous LaFeO3 Thin Film Chemiresistors Performances with Enhanced Gas Sensing. *ACS Appl. Mater. Interfaces* **2014**, *6*, 16217−16226.
(19) Wang, D.; Zhen, Y.; Xue, G.; Fu, F.; Liu, X.; Li, D. Synthesis of Mesoporous Bi2WO6 Architectures and Their Gas Sensitivity to Ethanol. *J. Mater. Chem. C* **2013**, *1*, 4153.
(20) Jaisutti, R.; Kim, J.; Park, S. K.; Kim, Y.-H. Low-Temperature Photochemically Activated Amorphous Indium-Gallium-Zinc Oxide for Highly Stable Room-Temperature Gas Sensors. *ACS Appl. Mater. Interfaces* **2016**, *8*, 20192−20199.
(21) Natile, M. M.; Ponzoni, A.; Concina, I.; Glisenti, A. Chemical Tuning versus Microstructure Features in Solid-State Gas Sensors: LaFe1-xGaxO3, a Case Study. *Chem. Mater.* **2014**, *26*, 1505−1513.
(22) Zhu, L.; Wang, Y.; Zhang, D.; Li, C.; Sun, D.; Wen, S.; Chen, Y.; Ruan, S. Gas Sensors Based on Metal Sulfide $Zn_{1-X}Cd_XS$ Nanowires with Excellent Performance. *ACS Appl. Mater. Interfaces* **2015**, *7*, 20793−20800.
(23) Chen, I.-C.; Lin, S.-S.; Lin, T.-J.; Hsu, C.-L.; Hsueh, T. J.; Shieh, T.-Y. The Assessment for Sensitivity of a NO2 Gas Sensor with ZnGa2O4/ZnO Core-Shell Nanowires-a Novel Approach. *Sensors* **2010**, *10*, 3057−3072.
(24) Men, H.; Gao, P.; Zhou, B.; Chen, Y.; Zhu, C.; Xiao, G.; Wang, L.; Zhang, M. Fast Synthesis of Ultra-Thin ZnSnO3 Nanorods with High Ethanol Sensing Properties. *Chem. Commun.* **2010**, *46*, 7581.
(25) Wang, S.; Zhang, J.; Yang, J.; Gao, X.; Zhang, H.; Wang, Y.; Zhu, Z. Spinel ZnFe2O4 Nanoparticle-Decorated Rod-like ZnO Nano-heterostructures for Enhanced Gas Sensing Performances. *RSC Adv.* **2015**, *5*, 10048−10057.
(26) Zhang, G.-Y.; Guo, B.; Chen, J. MCo2O4 (M=Ni, Cu, Zn) Nanotubes: Template Synthesis and Application in Gas Sensors. *Sens. Actuators, B* **2006**, *114*, 402−409.
(27) Li, L.; Zhang, C.; Chen, W. Fabrication of SnO_2−SnO Nanocomposites with P−n Heterojunctions for the Low-Temperature Sensing of NO_2 Gas. *Nanoscale* **2015**, *7*, 12133−12142.
(28) Bhardwaj, M.; Suryawanshi, A.; Fernandes, R.; Tonda, S.; Banerjee, A.; Kothari, D.; Ogale, S. CuCo2O4 Nanowall Morphology as Li-Ion Battery Anode: Enhancing Electrochemical Performance through Stoichiometry Control. *Mater. Res. Bull.* **2017**, *90*, 303−310.
(29) Ning, R.; Tian, J.; Asiri, A. M.; Qusti, A. H.; Al-Youbi, A. O.; Sun, X. Spinel CuCo2O4 Nanoparticles Supported on N-Doped Reduced Graphene Oxide: A Highly Active and Stable Hybrid Electrocatalyst for the Oxygen Reduction Reaction. *Langmuir* **2013**, *29*, 13146−13151.
(30) Amri, A.; Jiang, Z.-T.; Bahri, P. A.; Yin, C.-Y.; Zhao, X.; Xie, Z.; Duan, X.; Widjaja, H.; Rahman, M. M.; Pryor, T. Surface Electronic Structure and Mechanical Characteristics of Copper-Cobalt Oxide Thin Film Coatings: Soft X-Ray Synchrotron Radiation Spectroscopic Analyses and Modeling. *J. Phys. Chem. C* **2013**, *117*, 16457−16467.
(31) Zhou, J.; Zhang, J.; Rehman, A. U.; Kan, K.; Li, L.; Shi, K. Synthesis, Characterization, and Ammonia Gas Sensing Properties of Co3O4@CuO Nanochains. *J. Mater. Sci.* **2017**, *52*, 3757−3770.
(32) Paknahad, P.; Askari, M.; Ghorbanzadeh, M. Characterization of Nanocrystalline CuCo2O4 Spinel Prepared by Sol−gel Technique Applicable to the SOFC Interconnect Coating. *Appl. Phys. A* **2015**, *119*, 727−734.
(33) Serov, A.; Andersen, N. I.; Roy, A. J.; Matanovic, I.; Artyushkova, K.; Atanassov, P. CuCo2O4 ORR/OER Bi-Functional Catalyst: Influence of Synthetic Approach on Performance. *J. Electrochem. Soc.* **2015**, *162*, F449−F454.
(34) Stoyanova, D.; Christova, M.; Dimitrova, P.; Marinova, J.; Kasabova, N.; Panayotov, D. Copper-Cobalt Oxide Spinel Supported on High-Temperature Aluminosilicate Carders as Catalyst for CO-O2 and CO-NO Reactions. *Appl. Catal. B Environ.* **1998**, *17*, 233−244.
(35) Kim, H.-J.; Lee, J.-H. Highly Sensitive and Selective Gas Sensors Using P-Type Oxide Semiconductors: Overview. *Sens. Actuators, B* **2014**, *192*, 607−627.
(36) Chen, H.-Y.; Chen, J.-H. Preparation of P-Type CuCo2O4 Thin Films by Sol-Gel Processing. *Mater. Lett.* **2017**, *188*, 63−65.
(37) Huixia, L.; Yong, L.; Yanni, T.; Lanlan, L.; Qing, Z.; Kun, L.; Hanchun, T. Room Temperature Gas Sensing Properties of Tubular Hydroxyapatite. *New J. Chem.* **2015**, *39*, 3865−3874.
(38) Liu, S.; Zhang, S.; Xing, Y.; Wang, S.; Lin, R.; Wei, X.; He, L. Facile Synthesis of Hierarchical Mesoporous CuxCo3-xO4 Nanosheets Array on Conductive Substrates with High-Rate Performance for Li-Ion Batteries. *Electrochim. Acta* **2014**, *150*, 75−82.
(39) La Rosa-Toro, A.; Berenguer, R.; Quijada, C.; Montilla, F.; Morallón, E.; Vázquez, J. L. Preparation and Characterization of Copper-Doped Cobalt Oxide Electrodes. *J. Phys. Chem. B* **2006**, *110*, 24021−24029.

DOI: 10.1021/acsomega.7b01958
ACS Omega 2018, 3, 1977−1982